Please cite the Published Version

Additional Information: This is an accepted manuscript of an article which appeared in final form in Separation and Purification Technology, published by Elsevier.

Data Access Statement: The data that has been used is confidential.

Enquiries:

If you have questions about this document, contact openresearch@mmu.ac.uk. Please include the URL of the record in e-space. If you believe that your, or a third party's rights have been compromised through this document please see our Take Down policy (available from https://www.mmu.ac.uk/library/using-the-library/policies-and-guidelines)

Polyethyleneimine NH2-UiO-66 nanofiller-based mixed matrix membranes for natural gas purification

Yuchen Cui [a, #], Xiaolei Cui [a, #], Lubomira Tosheva [b], Chunzheng Wang [a], Yongming Chai [a], Zixi Kang [c], Qiang Gao [d], Kun Wang [c], Zhihan Zhang [a], Hailing Guo [a*], Daohong Xia [a], Daofeng Sun [c]

[a] State Key Laboratory of Heavy Oil Processing, College of Chemical Engineering, China University of Petroleum (East China), Qingdao, Shandong 266580, P.R. China.

[b] Department of Natural Sciences, Manchester Metropolitan University, Chester Street, Manchester M1 5GD, UK.

[c] School of Materials Science and Engineering, China University of Petroleum (East China), Qingdao, Shandong 266580, P.R. China.

[d] School of Chemistry and Chemical Engineering, Qinghai Normal University, Xining 810008, P. R. China.

[#] These authors should be considered co-first authors.

[*] Corresponding author. guohl@upc.edu.cn (H. Guo)

Abstract

Effective separation of CO_2 from CH_4 is crucial for the purification of natural gas, which requires membrane materials with high permeability, selectivity, and stability of under high pressures. In this work, a high CO_2-affinity MOF-based nanofiller (P_{in}@NH2-UiO-66) was prepared and integrated in polyetherimide (PEI) to prepare mixed matrix membranes (MMMs) for enhanced CO_2/CH_4 separation capabilities. The P_{in}@NH2-UiO-66 nanofiller comprised an in situ-formed polyethyleneimine-NH2-UiO-66 composite prepared via a one-pot synthesis. The polyethyleneimine was covalently attached to the H2BDC-NH2 ligand allowing for a stronger integration within the PEI matrix. The polyethyleneimine affects the nucleation of MOF, leading to

miniaturization of the MOF particles. The smaller-sized filler is beneficial for improved interaction at the filler-matrix interface. The numerous amino functionalities grafted onto the NH_2-UiO-66 increased the CO_2 adsorption sites, thereby enhancing the affinity for CO_2. Owing to the improved interaction, the elevated CO_2 attraction, and the inherent properties of the porous NH_2-UiO-66, the fabricated MMMs preformed superior in separating CO_2/CH_4. The 30-P_{in}@NH_2-UiO-66-PEI membrane (containing 30 wt% nanofiller) exhibited a CO_2/CH_4 selectivity of 27.7 and a CO_2 permeability of 2498.9 Barrer. The CO_2 permeability was 21 times greater than that of the pristine PEI membrane, and 4 times higher compared to P@NH_2-UiO-66 MMM with polyethyleneimine modified MOF filler prepared by a traditional wet impregnation method. Additionally, the novel MMM demonstrates excellent separation stability under conditions that mimic industrial settings, demonstrating its potential application for natural gas purification.

Keywords: Mixed-matrix membrane; NH_2-UiO-66; MOF nano-filler modification; CO_2 separation; in situ formation

1. Introduction

Recently, the development of technologies for CO_2 separation from natural gas has attracted considerable attention [1, 2]. The membrane separation technique [3-5] is recognized as one of the most feasible strategies to purify natural gas [6, 7], due to the minimal operational expenses, energy-efficient operation, and decreased carbon emissions. Industrial membranes for natural gas purification should operate effectively at temperatures of about 50 °C (the outlet temperature of a natural gas pipeline) and at elevated gas pressures, and consistently maintain high CO_2 permeability, selectivity and stability [2, 8]. Polymeric membranes currently predominate the membrane market due to their low cost and large-scale manufacturing. The cellulose acetate membrane developed by UOP is the most widely used membrane material in all membrane natural gas processing plants, with a selectivity of 10−15 [9]. However, there are several issues with acid cellulose membranes, including susceptibility to hydrolysis, inadequate permeability and selectivity. Freshly-made thin composite membranes often lose 25%

of their permeability within a week. The balance between permeability and selectivity of polymeric membranes remains challenging, along with maintaining the membrane's structural stability for effective CO_2 separation [10-12]. To tackle these challenges, diverse permeable fillers have been integrated into the polymer matrix to create mixed matrix membrane (MMM) [13-15].

In MMMs, the porous filler is crucial for enhancing CO_2 separation performance by creating pathways for low-resistance transport [15-19]. Among these fillers, metal-organic frameworks (MOFs) stand out as auspicious options, ascribed to the large surface areas and controllable porosity for CO_2 separation [20, 21]. However, improving interaction at the filler-matrix interface is challenging due to the intrinsic differences between organic polymers and MOFs. Moreover, the CO_2-binding property of the MOF fillers exerts a significant role in determining membrane performance. Therefore, it is essential to design MOF fillers that possess superior CO_2 adsorption properties and exhibit strong affinity with the polymer matrix [22].

Plenty research have been dedicated to directed towards advancing the performance of new-generation membranes by tuning the chemical affinity towards CO_2 [14, 23-28]. Amines interacting with open metal sites in MOFs effectively boost the CO_2 uptake at low pressures via furnishing extra adsorption sites [20, 29]. Polyethyleneimine stands out as a highly suitable choice for improving the CO_2 adsorption capabilities of MOFs, as it is rich in amino groups, particularly the primary amine sites located at the chain ends [26, 30, 31]. Additionally, the combination of organic polyethyleneimine and MOF materials is beneficial for enhanced interaction at the filler-matrix interface [28, 32].

The wet impregnation approach is a conventional method used to modify MOFs with polyethyleneimine. This approach involves the coupling of polyethyleneimine with the metal sites of the MOF through weak binding interactions. Liu et al. synthesized branched polyethyleneimine-functionalized UiO-66 via the wet impregnation approach [32], which served as filler in 6FDA-ODA to prepare MMMs for CO_2/CH_4 separating. This resulted in an enhanced CO_2/CH_4 selectivity of 56.49. In addition, the same group designed a nanocomposite filler (UiO-66-PEI@bmim[Tf_2N]) using UiO-66 decorated

84   with branched polyethyleneimine via wet impregnation method [33], and the MMMs

85   prepared showed an optimum CO_2/CH_4 selectivity of 59.99. Although

86   polyethyleneimine-modified MOF fillers enhance the separation performance of

87   MMMs, the preparation process of modified MOF fillers usually involves high-

88   temperature anhydrous and oxygen-free environment, which complicates the

89   membrane preparation process. Furthermore, a higher level of amine functionalization

90   would result in a higher CO_2 adsorption as well as an enhanced CO_2 permeance.

91   Notably, in comparison with the wet impregnation technique, the in situ covalent

92   grafting method employs a stronger force, consequently facilitating the filler's ability

93   to bind to a greater number of amino groups. Therefore, seeking a simple strategy to

94   modify MOF fillers by introducing more amino groups without high-temperature

95   processing can significantly reduce operational steps and energy consumption.

96   Herein, we propose a simple in situ one-pot synthesis strategy for the fabrication of

97   polyethyleneimine-modified NH_2-UiO-66 (P_{in}@NH_2-UiO-66) (Scheme 1). The

98   P_{in}@NH_2-UiO-66 nanofillers were then physically blended with polyetherimide to

99   prepare mixed matrix membranes with an enhanced CO_2 separation performance

100   compared to P@NH_2-UiO-66 fillers prepared by conventional wet impregnation.

101   During the in situ synthesis process, polyethyleneimine and H_2BDC-NH_2 ligands are

102   covalently linked to form nano-sized P_{in}@NH_2-UiO-66 fillers with a higher loading of

103   polyethyleneimine. In contrast, the wet impregnation method relies on weaker

104   interactions between NH_2-UiO-66 and polyethyleneimine, resulting in a lower loading

105   capacity of polyethyleneimine. Nano-fillers with high polyethyleneimine load and

106   small size should have better interfacial compatibility with the polymer matrix and

107   higher CO_2 adsorption capacity. Benefiting from these features of P_{in}@NH_2-UiO-66,

108   the MMMs exhibited outstanding CO_2/CH_4 separation performance. The 30-P_{in}@NH_2-

109   UiO-66-PEI membrane with a 30 wt% of the fillers had a CO_2 permeability of 2498.9

110   Barrer and a CO_2/CH_4 selectivity of 27.7, with 4 times greater permeability compared

111   to MMMs prepared using conventional wet impregnation P@NH_2-UiO-66 fillers.
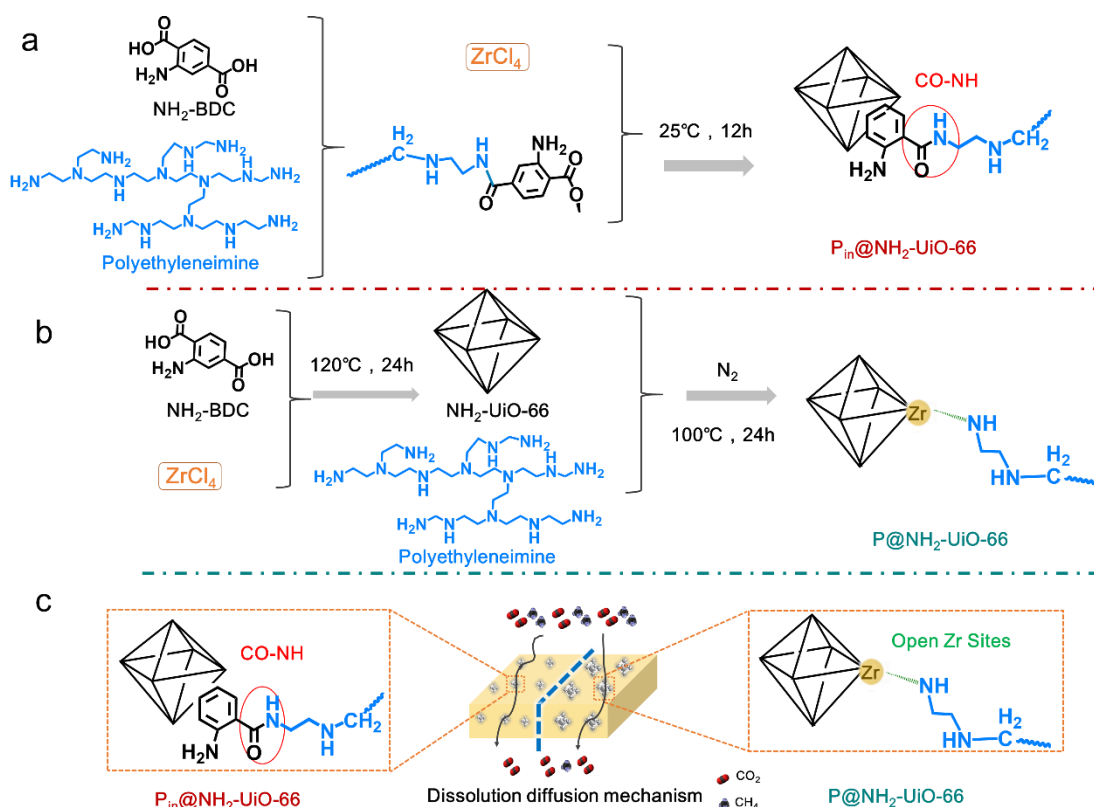
Scheme 1: Schematic illustration for the two preparation methods of mixed-matrix membranes in this work: (a) P_{in}@NH$_2$-UiO-66 in situ one-pot fabrication process, (b) P@NH$_2$-UiO-66 wet impregnation synthesis process, (c) membrane processing.

2. Experimental

2.1. Materials

Zirconium (IV) chloride (ZrCl$_4$, 99.5%) powder, formic acid (HCOOH, 88%) and dichloromethane (CH$_2$Cl$_2$, 99%) were supplied by Aladdin Biochemical Technology Co., Ltd. (China, Shanghai). 2-Aminoterephthalic acid (H$_2$BDC-NH$_2$, 98%) was sourced by Shanghai Macklin Biochemical Co., Ltd, N, N-Dimethylformamide (DMF, 99.8%), Ethanol (CH$_3$CH$_2$OH, AR) and methanol (CH$_3$OH, 99.7%) were supplied by Sinopharm Chemical Reagent Co., Ltd. Polyethyleneimine (99%, W.M. =10000) was supplied by Arkema, France. CH$_4$ and CO$_2$ (99.999%) were acquired from Nanjing Special Gases Company. Polyetherimide (PEI) was obtained from SABIC. All compounds employed as received without any other processing.

2.2. Synthesis of NH$_2$-UiO-66, P@NH$_2$-UiO-66 and P_{in}@NH$_2$-UiO-66 nano-fillers

The synthesis of NH$_2$-UiO-66 was conducted in accordance with established protocols

from previous studies [34]. A mixture of ZrCl$_4$ (4.91 mmol, 1.16 g) and 2-aminoterephthalic acid (4.91 mmol, 0.89 g) was disbursed in 55 mL of dimethylformamide. Subsequently, the mixture was elevated to 120 °C and maintained for 24 h. The obtained NH$_2$-UiO-66 yellow solid was isolated by centrifugation with dimethylformamide, methyl alcohol and DI water at 5000 rpm for 10 minutes. Afterward, the powder was activated at 60 °C to remove any remaining solvent.

The obtained NH$_2$-UiO-66 was modified with polyethyleneimine using a wet impregnation method. To eliminate coordinated water, NH$_2$-UiO-66 particles were heated at 150 °C overnight. Next, 30 mg of polyethyleneimine and 240 mg of NH$_2$-UiO-66 were separately disbursed in 24 mL methanol under sonication for 10 min. The NH$_2$-UiO-66 solution was then disbursed to the polyethyleneimine solution slowly while being sonicated. The mixture solution was agitated at 100 °C for 12 hours within a nitrogen environment. Subsequently, the articles were centrifuged and cleaned with absolute ethanol to eliminate solvents. The obtained product called P@NH$_2$-UiO-66 was dried at 110 °C for 12 h.

Based on the room temperature synthesis of NH$_2$-UiO-66 [35], 17.5 mL HCOOH was pre-mixed with 160 mL deionized (DI) water containing 1.16 g ZrCl$_4$ under agitation for 15 min. Following this, an additional 0.1 g of polyethyleneimine was incorporated into 50 mL of ethanol with 0.95 g of H$_2$BDC-NH$_2$. The blend was then thoroughly mixed for 12 hours at ambient temperature. Upon completion of mixing, a pinkish solid was obtained through centrifugal separation and was further purified by washing with ethanol and deionized water to eliminate contaminants. The product called P$_{in}$@NH$_2$-UiO-66 was obtained after drying. NH$_2$-UiO-66 was prepared in the same way but without the addition of polyethyleneimine and the product was called NH$_2$-UiO-66-RT.

2.3. Fabrication of MMMs

0.5g Polyetherimide was added to 4.5 g CH$_2$Cl$_2$ at room temperature. Following this, the MOF fillers (P@NH$_2$-UiO-66 and P$_{in}$@NH$_2$-UiO-66) were ground and dispersed into the solution to yield a filler content from 10 to 40 wt%. Subsequently, the combined process of 10 minutes of mechanical agitation and ultrasonic treatment were adopted. The casting solutions were subsequently spread onto a clean glass substrate using an automatic membrane applicator to regulate the membrane thickness. Following the application, CH$_2$Cl$_2$ solvent was allowed to evaporate completely at ambient condition

for 24 h, followed by additional evaporation periods at 60 °C and 120 °C for 24 h each. Once the solvent was evaporated, the prepared mixed matrix membranes (MMMs) were meticulously stripped from the glass surface. All membranes were reactivated at 120 °C for 24 h prior to gas permeability tests. P@NH$_2$-UiO-66-based and P$_{in}$@NH$_2$-UiO-66-based membranes with different MOFs loadings were labelled as wt%-P@NH$_2$-UiO-66-PEI and wt%-P$_{in}$@NH$_2$-UiO-66-PEI, respectively. As a comparison, 30wt % NH$_2$-UiO-66 was added as a filler to PEI to make 30-NH$_2$-UiO-66-PEI membrane.

2.4. Characterization methods

The microstructure and size of the MOF fillers, with the surface properties of the membranes, were investigated using a scanning electron microscopy (SEM, JEOL-7900F) and a transmission electron microscopy (TEM, JEOL JEM-2100UHR). Additionally, X-ray powder diffraction (XRD, Bruker D8 Advance) and Fourier transform infrared (FTIR) spectrometry (Bruker Vertex 70V) were employed to analyze the crystallographic characteristics of both the MOF fillers and the membranes. X-Ray photoelectron spectroscopy (XPS) analysis was carried out via a PH 5000 Versaprobe spectrometer. A Quantachrome Autosorb IQ instrument was carried out to measure N$_2$ adsorption isotherms at −196 °C. The CO$_2$ adsorption capacities of MOFs and membranes were also measured by a Quantachrome, Auto sorb IQ instrument at 25°C. The CO$_2$ and CH$_4$ adsorption isotherms for the membranes were measured with the Micromeritics ASAP-2020 surface area analyzer at a temperature of 25°C. Thermogravimetric (TGA) and differential scanning calorimetry (DSC) analyses were conducted using NETZSCH (STA 449 F5) to assess the mass loss and glass transition temperature T$_g$ of MMMs, respectively. The nitrogen elemental analysis was performed with a Vario Elementar cube. The kinetic viscosity of the casting solutions was measured by Rheometer (Haake Mars 60).

2.5. Gas-separation tests

The membranes were integrated into a stainless-steel chamber for conditioning, prior to the gas separation experiments. The gas permeability of the membranes was determined using the Wicke-Kallenbach technique, maintaining a feed pressure of 1 bar and a delta pressure across the membrane of 1 bar. The inlet gas was f supplied at a rate of 100 mL min^{-1} (equivalent to 50 cm^3 min^{-1} for each of the binary gas mixtures). A

sweeping argon of 40 cm³ min⁻¹ was applied. For analyzing the composition of the permeated gases, a gas chromatography setup (456-GC, Scion) was employed. Average permeation data were calculated based on measurements from at least three different membranes. The permeability, which is also referred to permeance P_i in Barrer (1 Barrer $=1 \times 10^{-10}$ cm³ (STP)·cm·cm⁻² s⁻¹·cmHg⁻¹), was calculated using Equation (1) for the membranes:

$$P_i = \frac{10^{-10} l N_i}{A \Delta p_i} \qquad (1)$$

In the specified formula, N_i (cm³ (STP)·s⁻¹) is the permeate flux, l (cm) denotes the membrane thickness, Δp_i (cmHg) is the pressure difference across the membrane, and A (cm²) indicates the membrane area.

The separation factor ($\alpha_{i/j}$) of the membrane was calculated based on Equation (2):

$$\alpha_{i/j} = \frac{X_i / X_j}{Y_i / Y_i} \qquad (2)$$

Where X_i/X_j and Y_i/Y_j represent the volume fraction in the permeate gas and feed gas.

The solution-diffusion model was applied to study the gas permeance through the membranes. The calculation formula is shown in Equation (3):

$$P_i l = S_i \times D_i \qquad (3)$$

where the permeability ($P_i l$) is equal to the product of the solubility (S_i, mol m⁻³ Pa⁻¹) and the diffusivity (D_i, m² s⁻¹), and l is the thickness of membranes.

The S_i can be calculated by Equation (4):

$$S_i = \frac{C_i}{P} \qquad (4)$$

where C_i (mmol cm⁻³) and P are the adsorption amount of the membrane for component i and pressure, respectively. D_i was calculated according to Equation (3).

3. Results and discussion

3.1. NH₂-UiO-66, P@NH₂-UiO-66 and Pᵢₙ@NH₂-UiO-66 nano-fillers

3.1. NH$_2$-UiO-66, P@NH$_2$-UiO-66 and P$_{in}$@NH$_2$-UiO-66 nano-fillers

XRD analysis (Fig. 1a) showed that NH$_2$-UiO-66 and P@NH$_2$-UiO-66 samples exhibit characteristic peaks 7.3° and 8.4° two theta, matching well the simulated NH$_2$-UiO-66 XRD pattern documented in the previous research [36]. This suggested that the wet impregnation method used for synthesizing P@NH$_2$-UiO-66 preserves the crystalline arrangement of NH$_2$-UiO-66. In the case of P$_{in}$@NH$_2$-UiO-66 prepared by in situ, one-pot synthesis, the typical NH$_2$-UiO-66 peaks at 7.3° and 8.4° two theta were observed, together with an amorphous peak in the range 3-12° two theta, indicating the presence of polyethyleneimine in the composite. The crystallinity of NH$_2$-UiO-66 in P$_{in}$@NH$_2$-UiO-66 was calculated via the background constant method [37, 38]. The crystallinity of NH$_2$-UiO-66 was assessed to be 100%, and the relative crystallinity of P$_{in}$@NH$_2$-UiO-66 was found to be 60.4%. During the in situ preparation of P$_{in}$@NH$_2$-UiO-66, the introduction of polyethyleneimine interfered with the coordination between the carboxyl groups and the metal zirconium (Zr), thereby affecting the nucleation procedure of NH$_2$-UiO-66 and leading to a reduced crystallinity.

From the FTIR spectra (Fig. 1b), all samples exhibit a peak at 770 cm^{-1}, associated with the of the Zr-O vibration in NH$_2$-UiO-66. The -NH- vibration of polyethyleneimine can be seen at 3390 cm^{-1}, indicating the effective grafting of polyethyleneimine onto NH$_2$-UiO-66. In contrast to P@NH$_2$-UiO-66, new characteristic peaks of the amide bond appear in P$_{in}$@NH$_2$-UiO-66 at 1658 cm^{-1} [39] and 1593 cm^{-1} [33], primarily arising from the condensation reaction between the carboxyl group in H$_2$BDC-NH$_2$ and the amino group in polyethyleneimine [28, 39]. In P@NH$_2$-UiO-66, the amine groups can bind to open Zr sites as reported [33, 40], however, this interaction is relatively weak, resulting in only modest quantity of polyethyleneimine being grafted onto the NH$_2$-UiO-66. The robust interaction enables P$_{in}$@NH$_2$-UiO-66 to combine a greater quantity of polyethyleneimine compared to P@NH$_2$-UiO-66. The nitrogen content was determined by elemental analyzer to compare the polyethyleneimine content of the three samples. The nitrogen contents of P$_{in}$@NH$_2$-UiO-66, P@NH$_2$-UiO-66, and NH$_2$-

UiO-66 were 6.56%, 4.78%, and 4.51%, respectively, indicating that P_{in}@NH$_2$-UiO-66

binds enhanced polyethyleneimine compared to P@NH$_2$-UiO-66. The interaction was

further examined by XPS (Fig. 1 c and d). The N1s peaks at 400 eV and 401.8 eV

correspond to the -NH$_2$ and -NH groups of NH$_2$-UiO-66, respectively (Fig. 1c). The

emergence of a distinct peak at 399.3 eV in the XPS spectrum corresponds to the amide

bonds in P_{in}@NH$_2$-UiO-66 [41]. Further, the C1s XPS spectra (Fig. 1d) indicate that

NH$_2$-UiO-66 reveals three distinct peaks at 284.5eV, 286 eV and 288.5eV, which are

respectively belong to sp^2 C, C-N, and O-C-O groups. The C-N ratio of the two

composites increases compared with that of NH$_2$-UiO-66, with the C-N ratio in

P_{in}@NH$_2$-UiO-66 being higher, confirming that more polyethyleneimine is present in

P_{in}@NH$_2$-UiO-66. Additionally, the characteristic peak of amide carbon was observed

at 287.6 eV for P_{in}@NH$_2$-UiO-66 [42]. The XPS results show that there is a

condensation reaction between the amino functional group and the carboxyl functional

group to form an amide (-CO-NH-).
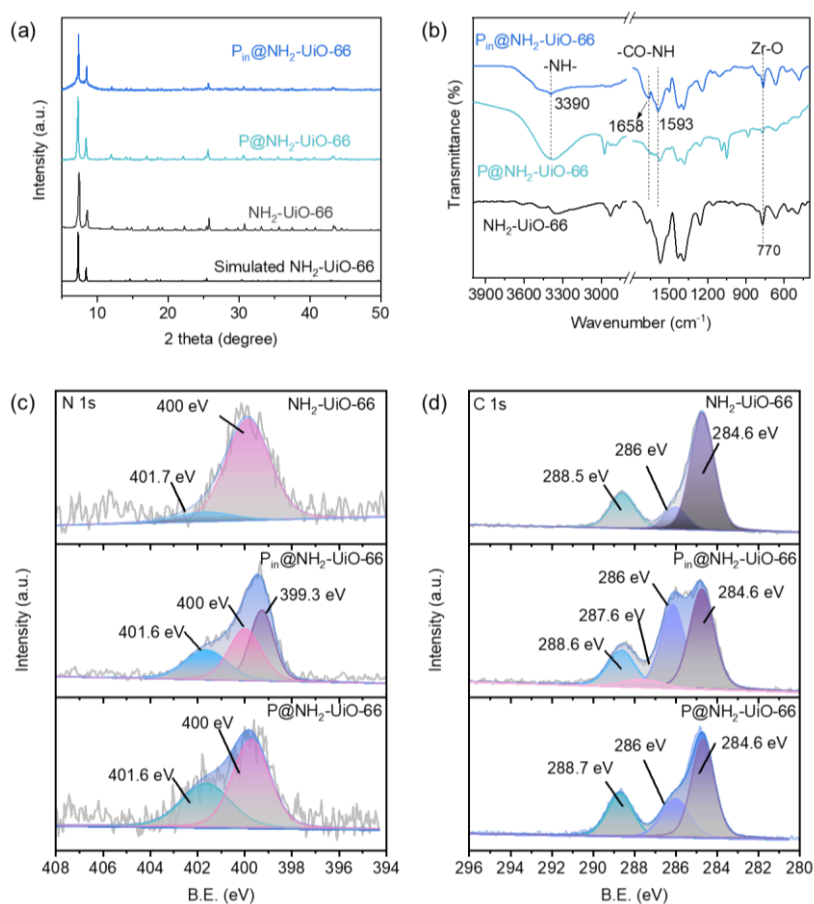
**Fig. 1.** (a) XRD, (b) FTIR, and (c) XPS N1s analysis and (d) XPS C1s analysis of the as-made NH$_2$-

259 UiO-66, P@NH$_2$-UiO-66, and P$_{in}$@NH$_2$-UiO-66 powders.

260 Fig. 2 exhibits the SEM and TEM images of the as-made NH$_2$-UiO-66, P@NH$_2$-UiO-

261 66 and P$_{in}$@NH$_2$-UiO-66 powders. The NH$_2$-UiO-66 nanoparticles exhibit dimensions

262 between 50 and 75 nm, exhibiting a cubic-like shape (Fig. 2a and d), while the P@NH$_2$-

263 UiO-66 are spherical with particle sizes around 100 nm (Fig. 2b and e). The differences

264 in the shape and size of P@NH$_2$-UiO-66 nanoparticles are considered to be a result of

265 the encapsulation of polyethyleneimine. The SEM image of NH$_2$-UiO-66-RT prepared

266 in the absence of polyethyleneimine indicates a cubic-like mosphology of this sample

267 with particle sizes of about 100 nm, and an XRD pattern that matches with the simulated

268 NH$_2$-UiO-66 (Fig. S1). Relatively, P$_{in}$@NH$_2$-UiO-66 consisted of significantly smaller

269 nanoparticles ($\sim$ 20 nm) (Fig. 2c and f). The condensation reaction to form amide groups

270 competes for the carboxyl group that should be coordinated with the metal Zr, thus

271 affecting the nucleation process of MOF and leading to the miniaturization of the MOF

272 particles [43]. The reduced particle size of the latter filler enhances the surface area and

273 could improve compatibility with the polymer matrix.
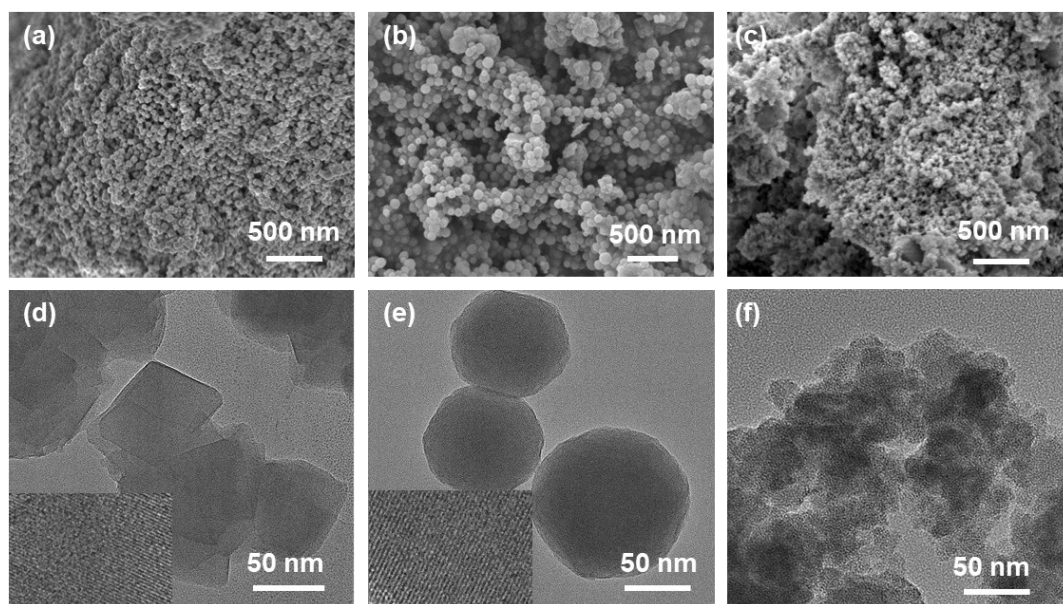
274

275 **Fig. 2.** SEM and TEM images of the as-made (a, d) NH$_2$-UiO-66, (b, e) P@NH$_2$-UiO-66, and (c, f)

276 P$_{in}$@NH$_2$-UiO-66. The lower left corner of d and e is a high-resolution image.

277 The N$_2$ adsorption isotherms of the NH$_2$-UiO-66, P@NH$_2$-UiO-66 and P$_{in}$@NH$_2$-UiO-

66 all followed hybrid type I and IV isotherms with H4 hysteresis (Fig. S2). Calculated by the t-plot method, the micropore volume of NH_2-UiO-66, P@NH_2-UiO-66 and P_{in}@NH_2-UiO-66 were 0.45 cm^3/g, 0.34 cm^3/g and 0.21 cm^3/g (Table S1). The pore size distribution reveals that the majority of pores measure approximately 0.4-0.6 nm and 1.1 nm. The latter represents the mesopores accumulated by micropores. There are also mesopores that are generated by nanoparticle accumulation in P_{in}@NH_2-UiO-66. While for the P@NH_2-UiO-66, the pore size distribution reveals lower value at around 1.1 nm, indicating less intra-particle mesopores. In addition, there were less mesopores that accumulated by the nanoparticles due to the larger particle size of P@NH_2-UiO-66. The mesopores allow rapid gas diffusion into the pores of fillers, further significantly decrease the trans-membrane mass transfer resistance of the MMMs, which facilitates diffusion processes. Therefore, the diffusion coefficient of P@NH_2-UiO-66-PEI membrane will be lower. The micropore diameters of NH_2-UiO-66 was 0.55 nm, being close to the MOF structure windows of about 6 Å, and the pore size of P@NH_2-UiO-66 and P_{in}@NH_2-UiO-66 reveal a slightly decrease (0.50 and 0.44 nm). The both reduction of pore volume and pore size indicates the occupation of the pores by polyethyleneimine. The P_{in}@NH_2-UiO-66 binds more polyethyleneimine than the P@NH_2-UiO-66, leading to more severe pore plugging.

The thermal stability of P@NH_2-UiO-66 and P_{in}@NH_2-UiO-66 was tested under N_2 atmosphere (Fig. 3). The initial mass decrement observed above 100 °C is assigned to the evaporation of adsorbed H_2O and gases. The step mass loss before 280 °C is attributed to dehydroxylation of the zirconium oxo clusters. The subsequent mass reduction occurring beyond 280 °C is ascribed to the structural collapse of NH_2-UiO-66 [35, 44]. These results show that the P@NH_2-UiO-66 and P_{in}@NH_2-UiO-66 fillers have good thermal stability.

303
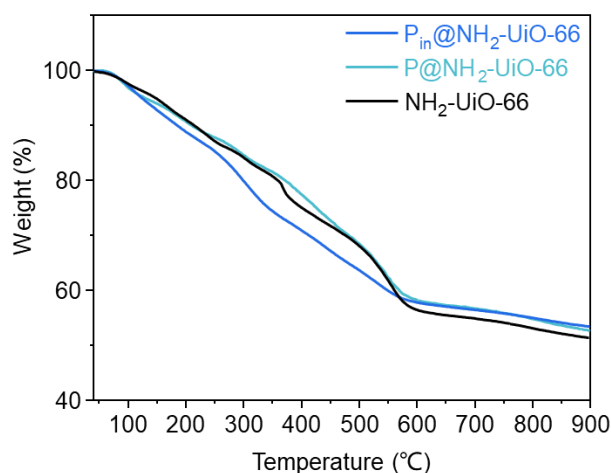
Fig. 3. TGA in N_2 of the as-made NH_2-UiO-66, P@NH_2-UiO-66, and P_{in}@NH_2-UiO-66.

305   P_{in}@NH_2-UiO-66 and P@NH_2-UiO-66 exhibited CO_2 saturation adsorption capacities

306   of 46 and 35 cm^3g^{-1}, respectively, surpassing that of NH_2-UiO-66 (15 cm^3g^{-1}) (Fig. 4).

307   The increase of CO_2 adsorption was mainly related to the modification of MOF by

308   polyethyleneimine. The grafting of polyethyleneimine with rich amino groups to NH_2-

309   UiO-66 generates additional sites for CO_2 adsorption. Furthermore, from the elemental

310   analysis and XPS results (Fig. 1c, d), P_{in}@NH_2-UiO-66 has a higher polyethyleneimine

311   content, therefore it has the highest CO_2 adsorption capacity. This high CO_2 adsorption

312   capacity is beneficial for the CO_2/CH_4 separation performance of the MMMs.

313
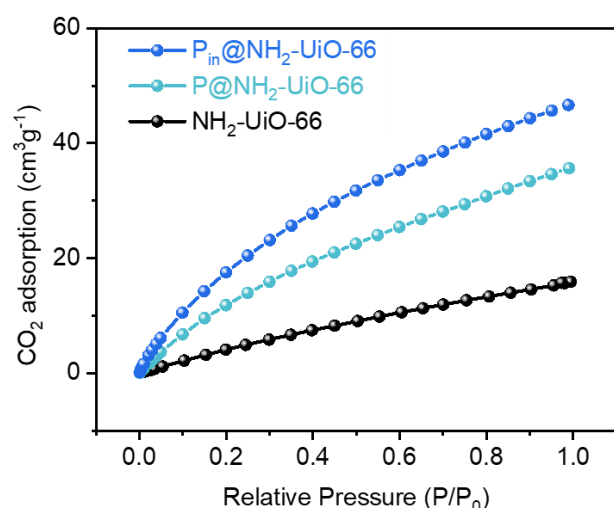
Fig. 4. The CO_2-adsorption curves of the as-made NH_2-UiO-66, P@NH_2-UiO-66, and P_{in}@NH_2-

315   UiO-66.

3.2. Membrane characterization

SEM images in Fig. 5, Fig. S3 and Fig. S4 were applied to characterize the top and cross-sectional structure of the pure PEI, P@NH$_2$-UiO-66-PEI, and P$_{in}$@NH$_2$-UiO-66-PEI membranes. The fabricated MMMs exhibited a substantial surface roughness, which tends to increase with the loading, compared to the PEI membrane (Fig. 5 a-c, Fig. S3 a-e and Fig. S4 a-d). Agglomeration was noticed on the surface of the P@NH$_2$-UiO-66-PEI membrane (Fig. 5c and Fig. S3), indicating a less-than-ideal distribution of particles throughout the PEI matrix. In the cross-section SEM images (Fig. S3 f-j and Fig. S4 f-j), the thickness of the PEI, P$_{in}$@NH$_2$-UiO-66-PEI, and P@NH$_2$-UiO-66-PEI membranes were determined to be in the range 68-91 μm. For P$_{in}$@NH$_2$-UiO-66-PEI, it is evident that P$_{in}$@NH$_2$-UiO-66 is enveloped by the polymer chains, forming defect-free microstructures (Fig. 5e and Fig. S4). The emergence of polymer veins serves as additional evidence supporting the existence of robust interfacial interactions [45], while this polymer vein was invisible in P@NH$_2$-UiO-66 based MMMs (The upper right corner of Fig. 5e and f). The outcome of this effect could be attributable to the presence of interaction forces between the imine groups (–N(R)-H) of the polyethyleneimine and the carbonyl groups (C=O) of the PEI matrix. The EDS mapping in Fig.5g-i shows that the nitrogen content of P$_{in}$@NH$_2$-UiO-66-PEI membrane is higher than that of P@NH$_2$-UiO-66-PEI and pure PEI membranes, further proving the nitrogen content of P$_{in}$@NH$_2$-UiO-66-PEI is the highest.
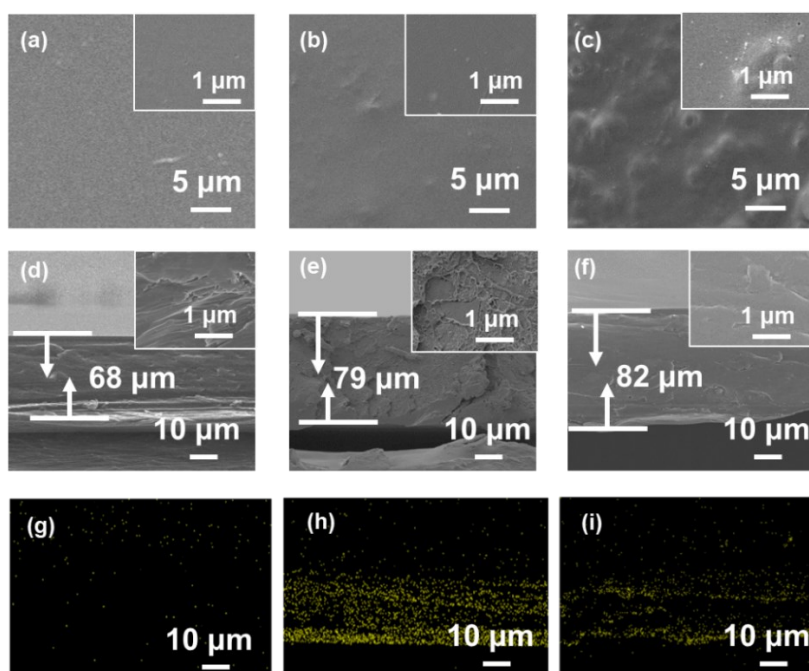
Fig. 5. Top-view SEM images of (a) pure PEI membrane, (b) 30-P$_{in}$@NH$_2$-UiO-66-PEI, (c) 20-P@NH$_2$-UiO-66-PEI, and cross-section SEM images of (d) pure PEI membrane, (e) 30-P$_{in}$@NH$_2$-UiO-66-PEI and (f) 20-P@NH$_2$-UiO-66-PEI (The upper right corner of a-f is the enlarged image), Corresponding elemental mapping images of N ka of (g) pure PEI membrane, (h) 30-P$_{in}$@NH$_2$-UiO-66-PEI, (i) 20-P@NH$_2$-UiO-66-PEI

XRD characterization was conducted to further characterize the structure of as-made membranes. Pristine PEI is a copolymer that features broad peaks centered at 14° two theta (Fig. 6a) [46]. The MOFs preserve their crystallinity and phase within the PEI as seen by the peaks at 7.37° and 8.44° two theta. Fig. S5 a, b displays the XRD patterns of P@NH$_2$-UiO-66-PEI and P$_{in}$@NH$_2$-UiO-66-PEI membranes prepared with different loadings. As the loading of the MOF increased, the intensity of the MOF characteristic peaks (especially at 7.37° and 8.44° two theta) progressively enhanced, indicating that the crystallinity of the nano-filler can be maintained during the membrane preparation process. The d-spacing values were calculated by using the Bragg's law. This value was lower for MMMs (d=5.7-5.9Å) than pristine PEI membrane (d=6.4 Å), as shown in the Fig .S5a, b. Thus form the result, the interaction between filler and polymer matrix increased the rigidity of the membrane, reducing the inter-segmental mobility and d-spacing, and enabling the membrane to allow only small molecules to penetrate through it. Given that the CO$_2$ molecule (3.6 Å) is smaller in size compared to the CH$_4$ molecule (3.8 Å), the MMMs potentially facilitates the passage of CO$_2$ through the membrane, thus enhancing CO$_2$ permeability.
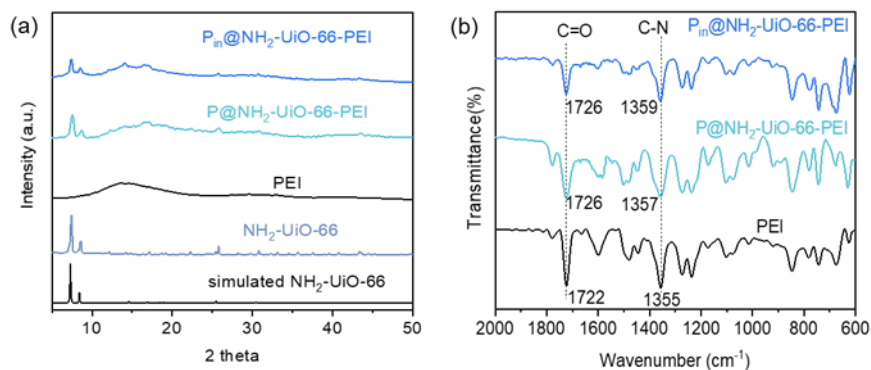

Fig. 6. XRD patterns (a) and FTIR spectra (b) of pristine PEI, P@NH$_2$-UiO-66-PEI and P$_{in}$@NH$_2$-

360 UiO-66-PEI membranes.

361 FTIR spectra of the membrane samples (Fig. 6b) were obtained to acquire insight of

362 the interaction between incorporated P@NH$_2$-UiO-66 or P$_{in}$@NH$_2$-UiO-66 MOFs and

363 PEI. The FTIR spectrum of the PEI matches with that described in published studies

364 [47]. The characteristic peaks corresponding to the pristine PEI polymer remain intact

365 in all MMMs, showing no noticeable changes in intensity. As the filler loading

366 increased, the peaks observed at 1780 cm^{-1} (C=O asymmetric), 1722 cm^{-1} (C=O

367 symmetric stretching vibration), and 1355 cm^{-1} (C-N stretch of imide groups) (Fig. S5

368 c, d), which were slightly red-shifted, and their intensity gradually increased. This could

369 be can be ascribed to the interaction between the amide groups and the carbonyl (C=O)

370 groups of the PEI via hydrogen bonding. P$_{in}$@NH$_2$-UiO-66-PEI exhibited enhanced

371 shift, suggesting significantly intensified hydrogen bonds.

372 The XRD pattern of 30-NH$_2$-UiO-66-PEI membrane matches with the simulated NH$_2$-

373 UiO-66 and pure PEI (Fig. S6). The top-view SEM images of 30-NH$_2$-UiO-66-PEI

374 indicates a rough surface morphology with particles agglomerated. The cross-section

375 SEM images shows obvious interface defects and voids, with membrane thickness of

376 59 μm.
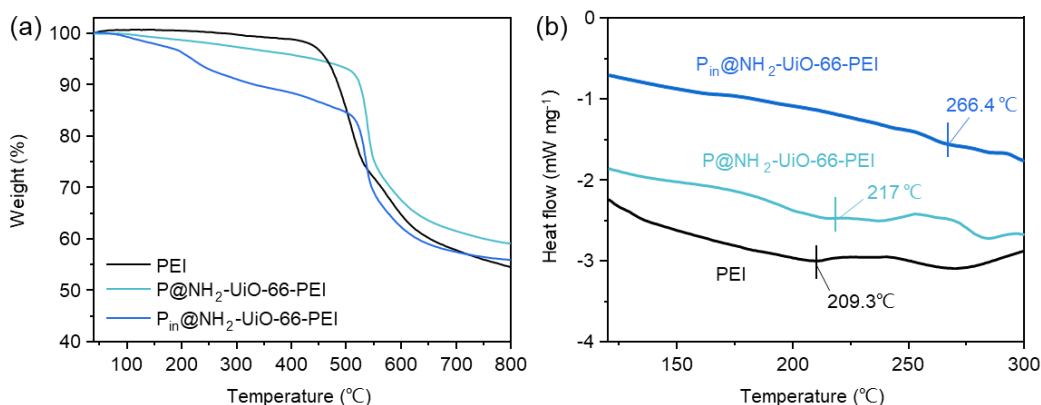
378 **Fig. 7.** TGA curves (a) and DSC curves (b) of pristine PEI, P@NH$_2$-UiO-66-PEI and P$_{in}$@NH$_2$-UiO-

379 66-PEI membranes.

380 The thermal stability of mixed matrix membranes was investigated using

381 thermogravimetric measurements (Fig. 7a). Starting from 200 °C, MMMs experienced

weight loss due to MOF degradation and the decomposing of polyethyleneimine of the fillers. The mass loss begin at 450-500 °C occurred as a result of PEI decarboxylation [46]. The MMMs with P_{in}@NH_2-UiO-66 and P@NH_2-UiO-66 fillers demonstrated a larger residual mass than the pristine PEI, suggesting filler decomposition. The glass transition temperature (T_g) determined by DSC measurements (Fig. 7b and Table.S2) was performed to assess the interaction between the fillers and the PEI. Pristine PEI membrane exhibited a T_g of 209.3 °C which matched well with the literature [48]. The 30-P_{in}@NH_2-UiO-66-PEI exhibited a much higher T_g value (266.4 °C) compared to 20-P@NH_2-UiO-66-PEI (217 °C). The reason is that more amine groups on the P_{in}@NH_2-UiO-66 show stronger hydrogen bonding with the PEI matrix, which indicates that P_{in}@NH_2-UiO-66-PEI have higher chain rigidity with robust interfacial interactions within the membranes. In addition, with the increase of filler content, the T_g of MMM increased, while the T_g of 40-P_{in}@NH_2-UiO-66-PEI membrane decreased slightly, which was due to the fact that overmuch filler was prone to agglomeration in the matrix and weakened the interfacial compatibility.

The viscosity of the casting solutions was measured to further investigate the interactions between the filler and the polymer (Fig. S7). The P_{in}@NH_2-UiO-66-PEI solution exhibited superior viscosity compared to that of the P@NH_2-UiO-66-PEI solution and the PEI polymer, confirming the enhanced interfacial compatibility [49, 50]. The enhanced interface compatibility is beneficial for the selective separation effect of CO_2.

3.3. Gas separation performance

Mixed gas permeation measurements (with CO_2/CH_4 =50/50 by volume) were performed to evaluate the separation capabilities of prepared membranes. Initially, the impact of P@NH_2-UiO-66 and P_{in}@NH_2-UiO-66 loading was examined. (Fig. 8a, b and Table S3). As exhibited in Table S3, the modified Zr-MOF MMMs exhibit higher CO_2 permeability and CO_2/CH_4 selectivity compared to NH_2-UiO-66-PEI. The aggregation caused by the larger crystal size of NH_2-UiO-66 and inhomogeneous distribution results in nonselective voids, leading to the lower selectivity for CO_2/CH_4.

411 And the low CO_2 saturated adsorption capacity of NH_2-UiO-66 leads to the lower CO_2

412 permeability. As the increase in both filler loadings, the CO_2 permeability increases,

413 mainly because the introduction of more MOFs provides more gas transport channels

414 for MMMs. Correspondingly, the CO_2/CH_4 selectivity demonstrated a tendency of

415 initial of incremental rise initially, which was succeeded by a decline. The increase of

416 polyethyleneimine load in the membrane introduced more CO_2 adsorption sites, which

417 resulted in higher gas selectivity. When the filler loading was too high, non-selective

418 voids were generated due to nanofiller aggregation (for instance Fig. S3h), reducing the

419 CO_2/CH_4 selectivity. For P_{in}@NH_2-UiO-66-PEI membrane, the MMM with 30% filler

420 loadings exhibited the best performance. The 30-P_{in}@NH_2-UiO-66-PEI membrane

421 exhibited the CO_2 permeability of 2498.9 Barrer with CO_2/CH_4 selectivity of 27.7,

422 respectively. The 20-P@NH_2-UiO-66-PEI demonstrated best results for the P@NH_2-

423 UiO-66 filler with a CO_2 permeability of 484.2 Barrer with CO_2/CH_4 selectivity of 11.4,

424 respectively. The significant difference in separation performance of P_{in}@NH_2-UiO-66

425 and P@NH_2-UiO-66 based membranes was mainly related to the amount of

426 polyethyleneimine modification. The membranes with higher polyethyleneimine

427 loading capacity showed superior CO_2/CH_4 separation performance.

428 Fig. 8c revealed that the incorporation of P@NH_2-UiO-66 and P_{in}@NH_2-UiO-66 nano-

429 fillers improved the selectivity and permeability for both gases over the pure PEI

430 membranes. The P_{in}@NH_2-UiO-66-PEI exhibited enhanced CO_2/CH_4 performance

431 compared to P@NH_2-UiO-66-PEI, which was due to the improved CO_2 affinity of

432 P_{in}@NH_2-UiO-66 and better interfacial compatibility the PEI matrix. The CO_2

433 permeability and CO_2/CH_4 selectivity of the 30-P_{in}@NH_2-UiO-66-PEI membrane was

434 respectively 4 and 2.7 times of the P@NH_2-UiO-66-PEI membrane and much higher

435 than the pure PEI membrane.
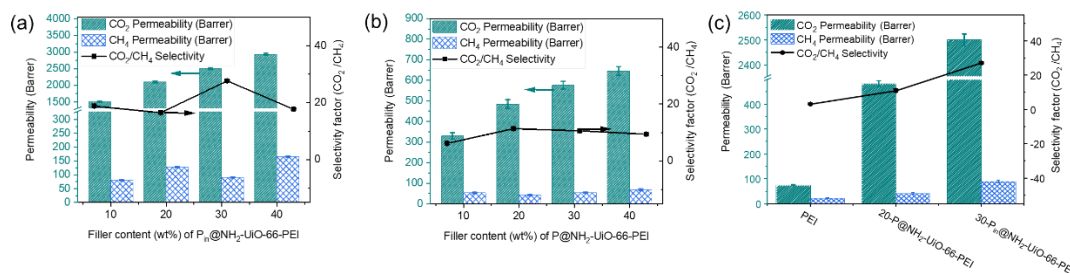
Fig. 8. The effect of fillers loading on the CO_2/CH_4 separation efficiencies of (a) $P_{in}NH_2$-UiO-66-PEI and (b) $P@NH_2$-UiO-66-PEI membranes. (c) Contrast of CO_2/CH_4 separation efficiencies of PEI, 20-$P@NH_2$-UiO-66-PEI and 30-$P_{in}NH_2$-UiO-66-PEI membranes.

To illustrate the improvement of CO_2 adsorption capacity of the membranes, the gas adsorption experiments were performed on the $P@NH_2$-UiO-66-PEI membrane and $P_{in}@NH_2$-UiO-66-PEI membrane with CO_2 and CH_4 at 298 K (Fig. S8). The adsorption capacities of the $P@NH_2$-UiO-66-PEI membrane for CO_2 and CH_4 were 10.20 and 3.31 $cm^3\ g^{-1}$ at 298 K, while those of $P_{in}@NH_2$-UiO-66-PEI membrane for CO_2 and CH_4 were 25.33 and 4.12 $cm^3\ g^{-1}$ at 298 K. The CO_2 adsorption ability of the $P_{in}@NH_2$-UiO-66-PEI membrane is higher than that of the $P@NH_2$-UiO-66-PEI membrane, proving that the in-situ modification of polyethyleneimine to the fillers can effectively improve the CO_2 adsorption capacity of the membrane. The solubility (S) and diffusivity (D) for the 30-$P_{in}@NH_2$-UiO-66-PEI and $P@NH_2$-UiO-66-PEI membranes are summarized in Table S4. The result shows that the selectivity of the membrane is more dependent on solubility (S_{CO2}/S_{CH4}=6.4 > D_{CO2}/D_{CH4}=4.3). It is much easier to adsorb CO_2 than CH_4 by the 30-$P_{in}@NH_2$-UiO-66 membranes, declining the adsorption and diffusion of CH_4, thereby enhancing the separation selectivity. The CO_2 solubility of 30-$P_{in}@NH_2$-UiO-66-PEI membrane shows higher value (1.2×10^{-8}> 8.2×10^{-9}) than 30-$P@NH_2$-UiO-66-PEI membrane due to the higher CO_2 adsorption ability of membrane. Furthermore, in contrast to the 30-$P_{in}@NH_2$-UiO-66-PEI membrane, the CO_2 diffusion of the 30-$P@NH_2$-UiO-66-PEI membrane shows lower value (5.3×10^{-6}< 1.1×10^{-5}), attributed to the reduced presence of mesopores in $P@NH_2$-UiO-66.

3.4. Influence of temperature, pressure, and feed gas

460   Fig. 9a assessed the impact of operational temperature within the range of 25–100 °C.

461   For 30-P_{in}@NH_2-UiO-66-PEI membrane, the permeability of CO_2 and CH_4 exhibited a

462   notable enhancement with increasing operational temperature, while the selectivity of

463   CO_2/CH_4 remained at a high level of 19.4. This shows that P_{in}@NH_2-UiO-66-PEI

464   membrane can maintain excellent CO_2/CH_4 separation performance even at high

465   operating temperatures (100 °C).

466   Examining the impact of transmembrane pressures on the performance of the produced

467   membranes is essential. The observed trend in Fig. 9b indicates that the CO_2

468   permeability gradually decreases with the transmembrane pressure increases from 1 bar

469   to 10 bar. This can be attributed to that the CO_2 affinity of the membrane approaches

470   saturation with the feed pressure increasing. As a result, the available sites for CO_2

471   adsorption become limited, leading to a decline in the overall permeability and

472   CO_2/CH_4 selectivity [11, 16]. The CO_2/CH_4 selectivity of the MMMs remains

473   substantially superior to that of the PEI membrane under elevated pressures (e.g. 10 bar,

474   Fig. 9b), emphasizing the enormous potential of these as-made MMMs under

475   operational conditions.

476   The different feed gas pressure of CO_2/CH_4 mixed gases (50/50, 30/70, and 10/90 by

477   volume) was investigated and the results are shown in Fig. 9c. The CO_2/CH_4 selectivity

478   decreased with the increase of CH_4 permeability due to higher CH_4 feed partial pressure.

479   30-P_{in}@NH_2-UiO-66-PEI still maintained the CO_2/CH_4 selectivity of 21.3 while a

480   permeability of up to 2116 Barrer in the case of a feed volume ratio of 10/90.

481
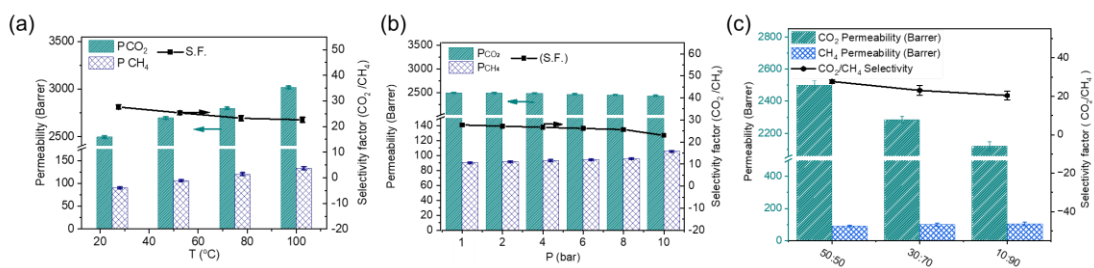
482   **Fig. 9.** (a)The effect of operation temperature on CO_2/CH_4 separation performance of 30-P_{in}@NH_2-

483   UiO-66-PEI at 1 bar. (b)The effect of operation pressures on CO_2/CH_4 separation performance of 30-

484   P_{in}@NH_2-UiO-66-PEI at 25 °C. (c) The effect of different feed gas ratios of the CO_2/CH_4 separation

485   performance of 30-P_{in}@NH_2-UiO-66-PEI at 25 °C and 1 bar.
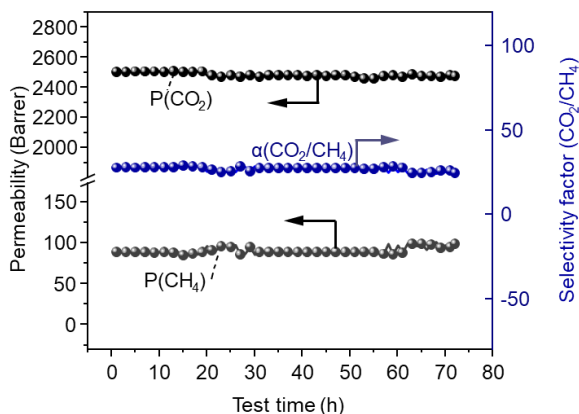
Fig. 10. 72 h operation test of 30-P_{in}@NH_2-UiO-66-PEI.

486

487

3.5. Long-term stability

488

489   Fig. 10 presents long-term stability test of CO_2/CH_4 separation to assess the stability of

490   the membrane structure. During a 72 h operation test, the 30-P_{in}@NH_2-UiO-66-PEI

491   membrane remained a stable CO_2 permeability of 2498.9 Barrer and a consistent

492   CO_2/CH_4 selectivity of 27.7. Additionally, it confirms that the fabricated 30-P_{in}@NH_2-

493   UiO-66-PEI membrane exhibited robust structural stability, indicating its potential

494   suitability for CO_2 capture from natural gas applications.

3.6. Simulation of industrial environment

495

496   To further simulate natural gas industrial conditions, we conducted tests to evaluate the

497   separation performance with feed gas CO_2: CH_4 = 10: 90 at various temperatures and

498   pressures (Table S5 and Table S6). The CO_2 permeability increases with increasing

499   temperature (25-50 °C) at 1 bar (Table S5). The CO_2 permeability reached 2363 Barrer

500   with the selectivity of 19.3 at 50 °C. As shown in Table. S6, when the pressure further

501   increased, the mixed-gas selectivity slightly decreased. The CO_2 permeability remained

502   at 2133 Barrer with CO_2/CH_4 selectivity of 15.1 at 50 °C and 10 bar, proving that the

503   P_{in}@NH_2-UiO-66-PEI membrane has excellent CO_2 permeability. MOFs-based

504   MMMs with mixed CO_2/CH_4 (volume ratio 10/90) reported in the literature are detailed

505   in Table S6, with 30-P_{in}@NH_2-UiO-66-PEI showing superior CO_2 permeability.

506 Therefore, the high-performance P_{in}@NH_2-UiO-66-PEI membrane holds significant

507 potential for industrial applications.

508 The 30-P_{in}@NH_2-UiO-66-PEI was subjected to a pressure of 60 bar for 3 hours using

509 a preforming machine to emulate the stability under high-pressure environment. A

510 comparison between the optical photographs and the surface SEM images of the

511 membrane taken before and after the application of pressure (Fig. S9). The membrane's

512 surface retained its initial morphology with some indentations and wrinkles after the

513 pressure exposure. Subsequently, the gas separation efficiency of mixed CO_2/CH_4

514 (volume ratio 10/90) of this membrane was tested at 50 °C and 10 bar, and the findings

515 indicated that the CO_2/CH_4 separation performance were maintained at a high level

516 (Table. S7).

517 *3.7. Comparison with upper bound*

518 Fig. 11 a shows the CO_2/CH_4 separation performances for the P_{in}@NH_2-UiO-66-PEI,

519 P@NH_2-UiO-66-PEI membranes compared with reported other state-of-the-art

520 functional groups modified MOFs MMMs and 2008 Robeson upper bounds. It can be

521 indicated that CO_2 permeability and CO_2/CH_4 selectivity of P_{in}@NH_2-UiO-66-PEI

522 exhibited significant enhancements compared to other functional group-modified

523 MOFs membranes. Moreover, Fig. 11 b and Table S7 illustrates the comparison of

524 P_{in}@NH_2-UiO-66-PEI and reported other MMMs that were measured with a mixed

525 feed gas of CO_2/CH_4=10/90. The P_{in}@NH_2-UiO-66-PEI membrane stands out due to

526 its exceptionally high CO_2 permeability compared to other membranes. In addition, 30-

527 P_{in}@NH_2-UiO-66-PEI demonstrated enhanced CO_2/CH_4 separation performance,

528 exceeding the upper bound established in 2008, demonstrating the developed

529 membrane with high potentiality for natural gas purification.
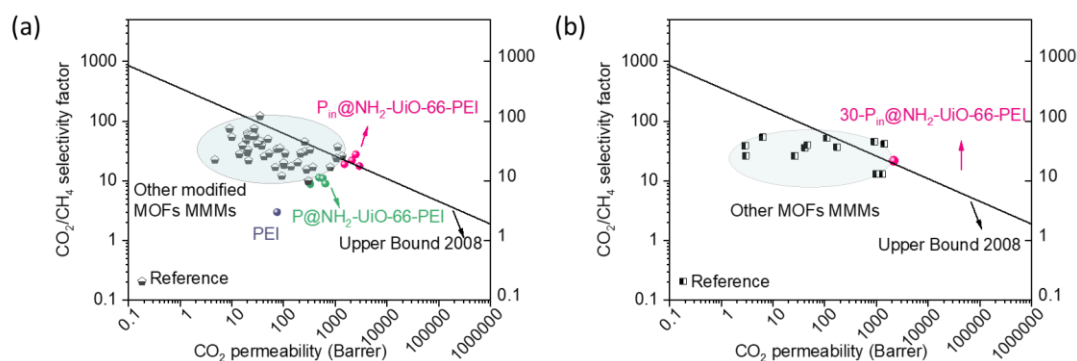
Fig. 11. Contrast of CO_2/CH_4 separation performances of 30-P_{in}@NH_2-UiO-66-PEI with (a) Robeson upper bound and other modified MOFs based MMMs, (b) other MOFs MMMs in feed gas CO_2/CH_4 =10/90.

Conclusions

In summary, this study reported the synthesis of polyethyleneimine-modified MOF fillers via an in situ one-pot method, and then incorporated into PEI to construct mixed matrix membranes for efficient CO_2/CH_4 separation. The separation performance of as-synthesized MMMs (P_{in}@NH_2-UiO-66-PEI) was also compared with that of MMMs with fillers prepared via conventional wet impregnation method (P@NH_2-UiO-66-PEI). Owing to the presence of polyethyleneimine in the in situ one-pot synthesis, P_{in}@NH_2-UiO-66 fillers have smaller particle size (~20 nm) and higher CO_2 adsorption capacity, improving the interfacial compatibility of MMM and the CO_2 transfer capability. The CO_2 permeability and CO_2/CH_4 selectivity of 30-P_{in}@NH_2-UiO-66-PEI MMMs (30 wt% loading) reached 2498.9 Barrer and 27.7, which were remarkably increased than that of pristine PEI membranes (75.1 Barrer and 3.3, respectively) and P@NH_2-UiO-66-PEI membranes (484.2 Barrer and 11.4, respectively). In addition, we simulated the industrial natural gas purification conditions (50 °C, 10 bar and CO_2: CH_4 = 10: 90 feed gas), and the P_{in}@NH_2-UiO-66-PEI membranes still have CO_2 permeability of 2133 Barrer and CO_2/CH_4 selectivity of 15.1 under these conditions. This study provides a novel perspective on the reasonable design of nano-fillers with unique properties and solve the interfacial compatibility of the MMMs for the development of natural gas purification membranes.

References

[1]   D. Jiménez-De-La-Cuesta, T. Mauritsen. Emergent constraints on Earth's transient and equilibrium response to doubled CO_2 from post-1970s global warming. Nature Geoscience, 12 (2019) 902-905. https://doi.org/10.1038/s41561-019-0463-y

[2]   R. W. Baker, B. Freeman, J. Kniep, X. Wei, T. Merkel. CO_2 capture from natural gas power plants using selective exhaust gas recycle membrane designs. International Journal of Greenhouse Gas Control, 66 (2017) 35-47. https://doi.org/10.1016/j.ijggc.2017.08.016

[3]   H. Zhai. Advanced Membranes and Learning Scale Required for Cost-Effective Post-combustion Carbon Capture. iScience, 13 (2019) 440-451. https://doi.org/10.1016/j.isci.2019.03.006

[4]   S. Zhou, O. Shekhah, A. Ramírez, P. Lyu, E. Abou-Hamad, J. Jia, J. Li, P. M. Bhatt, Z. Huang, H. Jiang, T. Jin, G. Maurin, J. Gascon, M. Eddaoudi. Asymmetric pore windows in MOF membranes for natural gas valorization. Nature, 606 (2022) 706-712. https://doi.org/10.1038/s41586-022-04763-5

[5]   I. Sullivan, A. Goryachev, I. A. Digdaya, X. Li, H. A. Atwater, D. A. Vermaas, C. Xiang. Coupling electrochemical CO_2 conversion with CO2 capture. Nature Catalysis, 4 (2021) 952-958. https://doi.org/10.1038/s41929-021-00699-7

[6]   Z. Liu, Y. Liu, W. Qiu, W. J. Koros. Molecularly Engineered 6FDA-Based Polyimide Membranes for Sour Natural Gas Separation. 59 (2020) 14877-14883. https://doi.org/https://doi.org/10.1002/anie.202003910

[7]   C. Ma, M. Wang, Z. Wang, M. Gao, J. Wang. Recent progress on thin film composite membranes for CO_2 separation. Journal of CO_2 Utilization, 42 (2020) 101296. https://doi.org/https://doi.org/10.1016/j.jcou.2020.101296

[8]   S. Miri, M. Omidkhah, A. Ebadi Amooghin, T. Matsuura. Membrane-based gas separation accelerated by quaternary mixed matrix membranes. Journal of Natural Gas Science and Engineering, 84 (2020) 103655. https://doi.org/10.1016/j.jngse.2020.103655

[9]   R. W. Baker, B. T. Low. Gas Separation Membrane Materials: A Perspective. Macromolecules, 47 (2014) 6999-7013. https://doi.org/10.1021/ma501488s

[10]   G. Liu, A. Cadiau, Y. Liu, K. Adil, V. Chernikova, I.-D. Carja, Y. Belmabkhout, M. Karunakaran, O. Shekhah, C. Zhang, A. K. Itta, S. Yi, M. Eddaoudi, W. J. Koros. Enabling Fluorinated MOF‐Based Membranes for Simultaneous Removal of H_2S and CO_2 from Natural Gas. Angew Chem Int Ed, 57 (2018) 14811. https://doi.org/10.1002/anie.201808991

[11]   X. Cai, Y. Yuan, M. Sheng, J. Wang, Z. Wang. High-performance CO_2/CH_4 separation membrane fabrication with PVAm modified by the MOFs containing amine groups. Journal of Natural Gas Science and Engineering, 89 (2021) 103874.

595   https://doi.org/10.1016/j.jngse.2021.103874

596   [12]   M. Costa Flores, K. C. D. S. Figueiredo. Asymmetric oxygen-functionalized carbon nanotubes

597   dispersed in polysulfone for CO_2 separation. J Appl Polym Sci, 140 (2022).

598   https://doi.org/10.1002/app.53303

599   [13]   C. Wu, K. Zhang, H. Wang, Y. Fan, S. Zhang, S. He, F. Wang, Y. Tao, X. Zhao, Y. B. Zhang, Y.

600   Ma, Y. Lee, T. Li. Enhancing the Gas Separation Selectivity of Mixed-Matrix Membranes Using

601   a Dual-Interfacial Engineering Approach. J Am Chem Soc, 142 (2020) 18503-18512.

602   https://doi.org/10.1021/jacs.0c07378

603   [14]   R. Ding, Q. Wang, X. Ruan, Y. Dai, X. Li, W. Zheng, G. He. Novel and versatile PEI modified

604   ZIF-8 hollow nanotubes to construct CO_2 facilitated transport pathway in MMMs. Sep Purif

605   Technol, 289 (2022) 120768. https://doi.org/10.1016/j.seppur.2022.120768

606   [15]   Q. Qian, P. A. Asinger, M. J. Lee, G. Han, K. Mizrahi Rodriguez, S. Lin, F. M. Benedetti, A. X.

607   Wu, W. S. Chi, Z. P. Smith. MOF-Based Membranes for Gas Separations. Chem Rev, 120 (2020)

608   8161-8266. https://doi.org/10.1021/acs.chemrev.0c00119

609   [16]   B. Chen, C. Wan, X. Kang, M. Chen, C. Zhang, Y. Bai, L. Dong. Enhanced CO_2 separation of

610   mixed matrix membranes with ZIF-8@GO composites as fillers: Effect of reaction time of ZIF-

611   8@GO. Sep Purif Technol, 223 (2019) 113-122. https://doi.org/10.1016/j.seppur.2019.04.063

612   [17]   P. Duan, J. C. Moreton, S. R. Tavares, R. Semino, G. Maurin, S. M. Cohen, K. Schmidt-Rohr.

613   Polymer Infiltration into Metal-Organic Frameworks in Mixed-Matrix Membranes Detected in

614   Situ by NMR. J Am Chem Soc, 141 (2019) 7589-7595. https://doi.org/10.1021/jacs.9b02789

615   [18]   A. R. Nabais, R. Ribeiro, J. Mota, V. D. Alves, I. Esteves, L. A. Neves. CO_2/N_2 Gas Separation

616   using Fe(BTC)-based Mixed Matrix Membranes: A view on the adsorptive and filler properties

617   of Metal-Organic Frameworks. Sep Purif Technol, 202 (2018) 174-184.

618   https://doi.org/10.1016/j.seppur.2018.03.028

619   [19]   S. Rafiq, M. Saeed, A. Jamil, M. I. Rashid, M. Irfan, T. Iqbal, A. Inayat, F. Jamil, J. Iqbal, M. S.

620   Khurram, M. S. Mehadi. Advances in Halloysite Nanotubes (HNTs)-Based Mixed-Matrix

621   Membranes for CO_2 Capture. ChemBioEng Reviews, 10 (2023) 480-490.

622   https://doi.org/https://doi.org/10.1002/cben.202200041

623   [20]   C. Song, R. Li, Z. Fan, Q. Liu, B. Zhang, Y. Kitamura. CO_2/N_2 separation performance of

624   Pebax/MIL-101 and Pebax/NH_2-MIL-101 mixed matrix membranes and intensification via sub-

625   ambient operation. Sep Purif Technol, 238 (2020) 116500.

626   https://doi.org/10.1016/j.seppur.2020.116500

627   [21]   S. Mutyala, M. Jonnalagadda, S. M. Ibrahim. Effect of modification of UiO-66 for CO_2

628   adsorption and separation of CO_2/CH_4. J Mol Struct, 1227 (2021) 129506.

629   https://doi.org/10.1016/j.molstruc.2020.129506

630   [22]   C. Ma, J. J. Urban. Hydrogen-Bonded Polyimide/Metal-Organic Framework Hybrid

631   Membranes for Ultrafast Separations of Multiple Gas Pairs. Advanced Functional Materials, 29

632   (2019). https://doi.org/10.1002/adfm.201903243

633   [23]   A. Atash Jameh, T. Mohammadi, O. Bakhtiari. Preparation of PEBAX-1074/modified ZIF-8

634   nanoparticles mixed matrix membranes for CO_2 removal from natural gas. Sep Purif Technol,

635   231 (2020) 115900. https://doi.org/10.1016/j.seppur.2019.115900

636   [24]   A. Jomekian, B. Bazooyar, R. M. Behbahani, T. Mohammadi, A. Kargari. Ionic liquid-modified

637   Pebax® 1657 membrane filled by ZIF-8 particles for separation of CO_2 from CH_4, N_2 and H_2.

638   J Membr Sci, 524 (2017) 652-662. https://doi.org/10.1016/j.memsci.2016.11.065

639 [25] M. Mirkovic, M. S. Yilmaz, L. Kljajevic, V. Pavlovic, M. Ivanovic, D. Djukic, T. Eren. Design
640 of PEI and Amine Modified Metakaolin-Brushite Hybrid Polymeric Composite Materials for
641 CO_2 Capturing. Polymers, 15 (2023). https://doi.org/10.3390/polym15071669

642 [26] X. Wang, Y. Wang, Y. Shan, X. Wang, Y. Yang, F. Zhang, X. Chen. Polyethyleneimine-modified
643 multi-walled carbon nanotubes mixed matrix membranes for CO_2/N_2 separation. Journal of
644 Environmental Chemical Engineering, 11 (2023) 109537.
645 https://doi.org/https://doi.org/10.1016/j.jece.2023.109537

646 [27] W. Wu, Z. Li, Y. Chen, W. Li. Polydopamine-Modified Metal-Organic Framework Membrane
647 with Enhanced Selectivity for Carbon Capture. Environ Sci Technol, 53 (2019) 3764-3772.
648 https://doi.org/10.1021/acs.est.9b00408

649 [28] J. Zhu, L. Wu, Z. Bu, S. Jie, B.-G. Li. Polyethyleneimine-Modified UiO-66-NH_2(Zr) Metal–
650 Organic Frameworks: Preparation and Enhanced CO_2 Selective Adsorption. ACS Omega, 4
651 (2019) 3188-3197. https://doi.org/10.1021/acsomega.8b02319

652 [29] Q. Zhao, Y. Sun, J. Zhang, F. Fan, T. Li, G. He, C. Ma. Mixed matrix membranes incorporating
653 amino-functionalized ZIF-8-NH_2 in a carboxylic polyimide for molecularly selective gas
654 separation. Journal of Membrane Science, 693 (2024).
655 https://doi.org/10.1016/j.memsci.2023.122326

656 [30] X. Guo, L. Ding, K. Kanamori, K. Nakanishi, H. Yang. Functionalization of hierarchically
657 porous silica monoliths with polyethyleneimine (PEI) for CO_2 adsorption. Microporous
658 Mesoporous Mater, 245 (2017) 51-57. https://doi.org/10.1016/j.micromeso.2017.02.076

659 [31] Y. Zhou, Y. Wang, Y. Wang, X. Li. Humidity-Enabled Ionic Conductive Trace Carbon Dioxide
660 Sensing of Nitrogen-Doped $Ti_3C_2T_x$ MXene/Polyethyleneimine Composite Films Decorated
661 with Reduced Graphene Oxide Nanosheets. Anal Chem, 92 (2020) 16033-16042.
662 https://doi.org/10.1021/acs.analchem.0c03664

663 [32] B. Liu, D. Li, J. Yao, H. Sun. Enhanced CO_2 selectivity of polyimide membranes through
664 dispersion of polyethyleneimine decorated UiO-66 particles. J Appl Polym Sci, 137 (2020).
665 https://doi.org/10.1002/app.49068

666 [33] B. Liu, D. Li, J. Yao, H. Sun. Improved CO_2 separation performance and interfacial affinity of
667 mixed matrix membrane by incorporating UiO-66-PEI@[bmim][Tf_2N] particles. Sep Purif
668 Technol, 239 (2020) 116519. https://doi.org/10.1016/j.seppur.2020.116519

669 [34] A. Micero, T. Hashem, H. Gliemann, A. Leon. Hydrogen Separation Performance of UiO-66-
670 NH_2 Membranes Grown via Liquid-Phase Epitaxy Layer-by-Layer Deposition and One-Pot
671 Synthesis. Membranes (Basel), 11 (2021). https://doi.org/10.3390/membranes11100735

672 [35] Z. Li, W. Zhang, M. Tao, L. Shen, R. Li, M. Zhang, Y. Jiao, H. Hong, Y. Xu, H. Lin. In-situ
673 growth of UiO-66-NH2 in porous polymeric substrates at room temperature for fabrication of
674 mixed matrix membranes with fast molecular separation performance. Chemical Engineering
675 Journal, 435 (2022). https://doi.org/10.1016/j.cej.2022.134804

676 [36] H. Molavi, A. Shojaei, S. A. Mousavi. Improving mixed-matrix membrane performance via
677 PMMA grafting from functionalized NH_2–UiO-66. Journal of Materials Chemistry A, 6 (2018)
678 2775-2791. https://doi.org/10.1039/c7ta10480d

679 [37] S. Basu, A. Cano-Odena, I. Vankelecom. Asymmetric Matrimid/[Cu_3(BTC)$_2$] mixed-matrix
680 membranes for gas separations. J Membr Sci, 362 (2010) 478-487.
681 https://doi.org/10.1016/j.memsci.2010.07.005

682 [38] S. Soheili, A. Nakhaei Pour, A. Mohammadi. SAPO-34 synthesis by combinations of structure-

683   directing agents: Experimental and Monte Carlo simulations studies. Microporous Mesoporous
684   Mater, 317 (2021). https://doi.org/10.1016/j.micromeso.2021.111003

685   [39]   J. Fang, L. Zhang, C. Li. Polyamide 6 composite with highly improved mechanical properties
686   by PEI-CNT grafted glass fibers through interface wetting, infiltration and crystallization.
687   Polymer, 172 (2019) 253-264. https://doi.org/10.1016/j.polymer.2019.03.013

688   [40]   Y. Lin, Q. Yan, C. Kong, L. Chen. Polyethyleneimine incorporated metal-organic frameworks
689   adsorbent for highly selective CO_2 capture. Sci Rep, 3 (2013) 1859.
690   https://doi.org/10.1038/srep01859

691   [41]   Z. B. Zhou, X. H. Han, Q. Y. Qi, S. X. Gan, D. L. Ma, X. Zhao. A Facile, Efficient, and General
692   Synthetic Method to Amide-Linked Covalent Organic Frameworks. J Am Chem Soc, 144 (2022)
693   1138-1143. https://doi.org/10.1021/jacs.1c12392

694   [42]   Q. Liang, M. Zhang, Z. Zhang, C. Liu, S. Xu, Z. Li. Zinc phthalocyanine coupled with UIO-66
695   (NH_2) via a facile condensation process for enhanced visible-light-driven photocatalysis. J
696   Alloys Compd, 690 (2017) 123-130. https://doi.org/10.1016/j.jallcom.2016.08.087

697   [43]   S. Diring, S. Furukawa, Y. Takashima, T. Tsuruoka, S. Kitagawa. Controlled Multiscale
698   Synthesis of Porous Coordination Polymer in Nano/Micro Regimes. Chem Mater, 22 (2010)
699   4531-4538. https://doi.org/10.1021/cm101778g

700   [44]   L. Chen, X. Ren, Y. Li, D. Hu, X. Feng, W. Li. Enhancing interface compatibility of UiO-66-
701   NH2 and polyamide by incorporating dopamine into thin film nanocomposite membranes. J
702   Membr Sci, 654 (2022) 120565. https://doi.org/10.1016/j.memsci.2022.120565

703   [45]   K. Chen, L. Ni, H. Zhang, L. Li, X. Guo, J. Qi, Y. Zhou, Z. Zhu, X. Sun, J. Li. Phenolic resin
704   regulated interface of ZIF-8 based mixed matrix membrane for enhanced gas separation. J
705   Membr Sci, 666 (2023) 121117. https://doi.org/10.1016/j.memsci.2022.121117

706   [46]   G. Yang, Y. Wang, M. Sun, P. Xu, C. Wang, K. Huang, H. Jiang, S. Mintova, H. Guo. Is amino-
707   modification of HKUST-1 in PEI mixed-matrix membranes always favorable to CO_2 separation?
708   Microporous Mesoporous Mater, 359 (2023) 112649.
709   https://doi.org/10.1016/j.micromeso.2023.112649

710   [47]   A. Choudhury. Dielectric and piezoelectric properties of polyetherimide/$BaTiO_3$
711   nanocomposites. Mater Chem Phys, 121 (2010) 280-285.
712   https://doi.org/10.1016/j.matchemphys.2010.01.035

713   [48]   Y. Wang, G. Yang, H. Guo, X. Meng, G. Kong, Z. Kang, R. Guillet-Nicolas, S. Mintova.
714   Preparation of HKUST-1/PEI mixed-matrix membranes: Adsorption-diffusion coupling control
715   of small gas molecules. J Membr Sci, 643 (2022) 120070.
716   https://doi.org/10.1016/j.memsci.2021.120070

717   [49]   E. D. Walter, D. Zhang, Y. Chen, K. Sung Han, J. D. Bazak, S. Burton, K. O'harra, D. W. Hoyt,
718   J. E. Bara, D. Malhotra, S. I. Allec, V. A. Glezakou, D. J. Heldebrant, R. Rousseau. Enhancing
719   CO_2 Transport Across a PEEK-Ionene Membrane and Water-Lean Solvent Interface.
720   ChemSusChem, 16 (2023) e202300157. https://doi.org/10.1002/cssc.202300157

721   [50]   Z. Dai, L. Deng. Membrane absorption using ionic liquid for pre-combustion CO_2 capture at
722   elevated pressure and temperature. International Journal of Greenhouse Gas Control, 54 (2016)
723   59-69. https://doi.org/10.1016/j.ijggc.2016.09.001